Analysis of He I 1083 nm Imaging Spectroscopy Using a Spectral Standard

E.V. Malanushenko
National Solar Observatory, P.O.Box 26732, Tucson, AZ 85726, U.S.A.

H.P. Jones
NASA'S GSFC

February 20, 2004

Abstract.

We develop a technique for the analysis of He I 1083 nm spectra which addresses several difficulties through determination of a continuum background by comparison with a well calibrated standard and through removal of nearby solar and telluric blends by differential comparison to an average spectrum. The method is compared with earlier analysis of imaging spectroscopy obtained at the National Solar Observatory/Kitt Peak Vacuum Telescope (NSO/KPVT) with the NASA/NSO Spectromagnetograph (SPM). We examine distributions of Doppler velocity and line width as a function of central intensity for an active region, filament, quiet Sun, and coronal hole. For our example, we find that line widths and central intensity are oppositely correlated in a coronal hole and quiet Sun. Line widths are comparable to the quiet sun in the active region, are systematically lower in the filament, and extend to higher values in the coronal hole. Outward velocities of ≈ 2 to 4 km/s are typically observed in the coronal hole. The sensitivity of these results to analysis technique is discussed.

Keywords: Solar Chromosphere, Coronal Hole, 1083 nm helium line

1. Introduction

Solar observations of the main spectral component of He I 1083 nm form a rich and extensive database for the study of solar activity and coronal holes. Whole-disk spectroheliograms of He I 1083 nm equivalent width from the National Solar Observatory/Kitt Peak Vacuum Telescope (NSO/KPVT; Livingston *et al.*, 1976) and, more recently, filtergrams from the High Altitude Observatory/Mauna Loa Observatory (Elmore *et al*, 1994) have revealed a wealth of observational phenomena. These include coronal hole identification and evolution (Harvey and Recely, 2002), relationship of X-ray bright points to He dark-points (Golub *et al.*, 1989), long - duration "flares" (Harvey, 1994), and identification of the He 1083 nm manifestations of Moreton or "EIT" waves (Gilbert and Holzer, 2002). Regular observations of 1083 nm spectroheliograms are now also obtained at the Crimean Astrophysical Observatory (Stepanian *et al.*, 2000).

However, more can be learned from spectrally resolved observations. He I 1083 nm absorption consists of a spectral triplet with rest wavelengths of 1083.0341 - (0.,0.0091,0.126) nm and respective statistical weights of g=(5,3,1). On the Sun only two spectral components are observed since the g=5 and g=3 lines are separated in wavelength by much less than their widths. The multiplet is formed in narrow regions near the interface between the chromosphere and transition region (TR) (Avrett, Fontenla, and Loeser, 1994; Andretta and Jones, 1997). In the upper chromosphere, the dominant process for populating the lower energy levels is photoionization - recombination (PR) driven by coronal and TR EUV radiation, while in the "cool" ($\approx$ 2 - 3 $\times 10^4$ K) TR, direct collisional excitation and ionization become important. Much of the observed variation in line strength (equivalent width or central line depth) is controlled by external radiation. In coronal holes the deficiency of coronal radiation weakens the lines, while in active regions and network boundaries enhanced coronal and particularly TR EUV radiation strengthen 1083 nm absorption. In all cases the source function in regions where PR is effective is determined almost entirely by scattered photospheric radiation and is insensitive to local thermodynamic conditions. In contrast to line strengths, the shape and spectral positions of the lines are mostly determined by local thermodynamic properties and flows in the regions of formation. Thus imaging spectroscopy, which spatially resolves variations in both strength and shape of the He I 1083 nm multiplet, is in principle a powerful tool for studying the chromosphere-TR interface at the base of different coronal and activity-associated structures.

Jones (2003; paper I) discusses many issues regarding the use and analysis of He I 1083 nm imaging spectroscopy and presents a rapid method for computing equivalent width, Doppler velocity, line width, central line depth, and asymmetry measures of the main spectral component. He notes that spectral analysis is difficult because the He I 1083 nm is weak, highly variable, and blended with numerous other telluric and solar lines. In particular, the spectral background for computing line profiles often cannot be reliably determined from observational data by conventional interpolation. True continuum windows to the solar spectrum are well removed from the centroid of the He I multiplet, lying beyond the bandpass limits or domains of linear spectral response of imaging instruments which can spectrally isolate and resolve the lines. The He I 1083 nm lines blend with "pseudo-continua" in the wings of the nearby Si I and water vapor lines in highly variable proportions. These wavelength domains are unstable references for finding the combined background of continuum and spectral blends. An extreme but commonly occurring example of this instability occurs at

spatial points where the line-of-sight velocity shifts the line absorption into a pseudo-continuum window (Jones, 1994). (Giovanelli and Hall, 1976) also discuss the sensitivity of He I 1083 nm reduction and analysis to choice of continuum and spectral blends and point out weak unidentified absorption features near the weak member of the multiplet.

In this paper, we present a new method for extracting the backgrounds of continuum radiation and spectral blends which is based on comparison of the observed spectra with a well-calibrated standard and which can be applied to the He I 1083 nm lines or, in principle, to observations of other spectral lines even when the above difficulties apply. We also present a least-squares fitting procedure for removing blends and deriving spectral properties which differs from the method presented in paper I and compare the two techniques on the same data set. Finally, we show and discuss the properties of He I 1083 nm line profiles in four different solar disk features.

2. Observations and Analysis

One of us (HJ) obtained imaging spectroscopy at 1083 nm of an area near Sun center including a coronal hole at the NSO/KPVT on 2000 April 17 using the NASA/NSO spectromagnetograph (SPM) (Jones *et al.*, 1992). The spectral dispersion of the observations was 0.083Å/pix, and the spectral range was about 1.7 nm, roughly centered around 1083 nm. The spatial scale was $1.10''$/pix. For improving signal to noise,

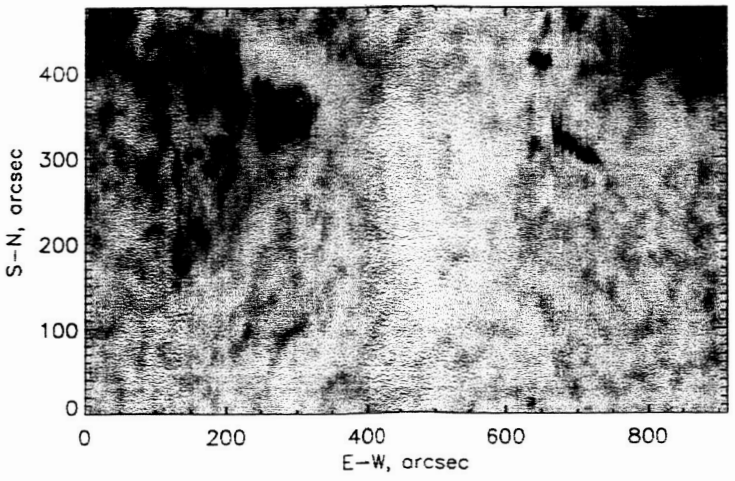

Figure 1. An image at the center of He 1083.0 nm, observed on KPVT with SPM 17 April 2000.

these spectra were averaged to a spatial scale of 2.68″/pix. An image of the line-center intensity of the He 1083.0 nm line is shown on Figure 1.

We performed dark and flat-field corrections using the technique presented in paper I. To form the flat field, we obtained an average spectrum while scanning the solar image parallel to the slit from limb to limb so that every spatial position along the exit slit received equal accumulated solar exposure. We then computed a sequence of least-squares fits to isolate and remove the spectral lines from the accumulated exposure. The remaining analysis differs from paper I.

To enable a comparison with a spectral standard, we used linear interpolation to shift and stretch SPM spectra at each spatial position to compensate for local solar velocities (primarily rotation and p-mode oscillations) and the variation of spectrograph dispersion with spatial position along the entrance slit. We determined the magnitudes of these corrections by requiring the central wavelengths of Gaussian fits to the cores of the solar lines Si I 1082.71 nm and Na I 1083.49 nm to be transformed to their average positions. Shifting the spectra to this local solar frame optimizes comparison with the solar portions of the spectral standard but introduces line shifts ($\approx \pm 0.3 pixels$) in the telluric lines which are essentially at rest in the observer's frame. We then normalized the observed spectra to a first approximation of the background continuum which we computed from linear least-squares fits to intensities in two continuum spectral zones around 1082.3 nm and 1083.6 nm. Comparison of the quiet-Sun spatial average of these "standardized" spectra (Avr in Figure 2a) with carefully calibrated observations (Wallace *et al.*, 1993; the "NSO Atlas") from the NSO/McMath-Pierce Fourier Transform Spectrometer (Atlas in Figure 2a) shows the SPM spectral response to be non-linear. Perhaps this is due to the SPM detector or residual errors in the flat-fielding process.

To account for this nonlinear spectral response, we adapted a procedure for correcting observed spectra using a well calibrated reference spectrum developed by (Malanushenko, Polosukhina and Weiss, 1992) with the NSO Atlas as the standard. The basic idea is to determine the non-linear response from ratios of observed to reference spectra in wavelength zones with low observed solar and instrumental variations. For our data, we performed this task in two stages. First, we normalized the *average* SPM spectrum to the standard to compensate for the different spectral resolutions of the observing and calibrating instruments. Then we compared individual spectra to the normalized average to separate non-linear spectral response from solar variations.

To derive a standard with the SPM spectral resolution, we computed the ratio of the SPM to NSO Atlas spectra (Figure 2.b). The ratio departs significantly from unity in regions near line centers because

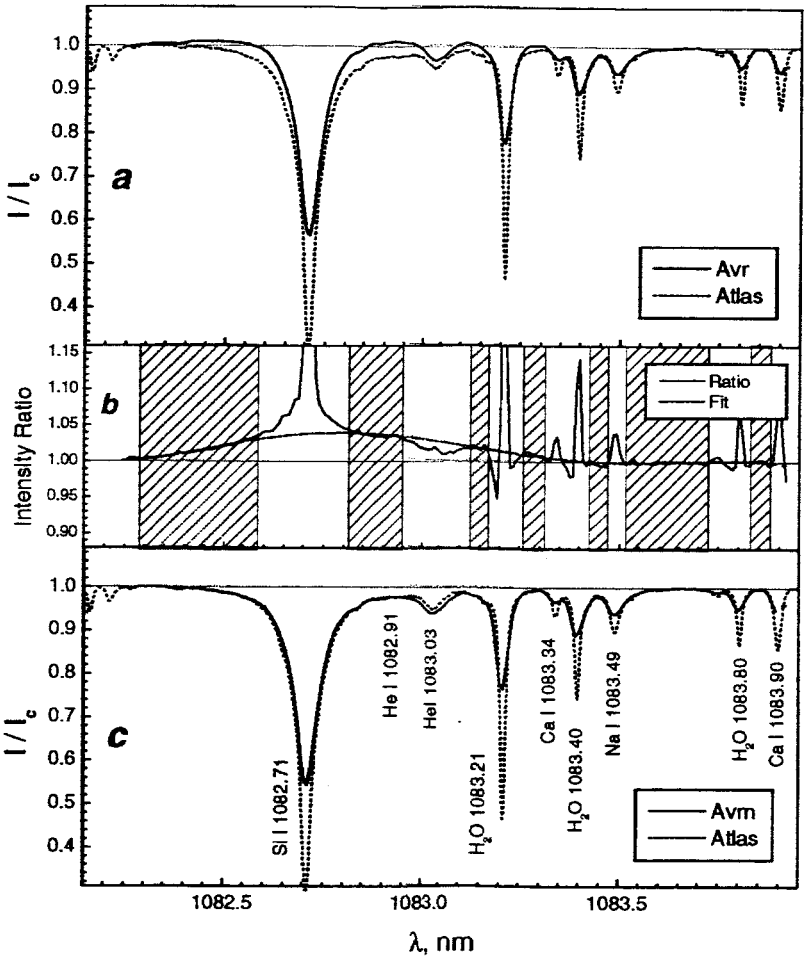

Figure 2. Normalization of average spectrum to reference spectrum to adjust for different spectral resolutions between different observing and calibrating instruments. Atlas refers to spectral standard, Avr to the SPM average spectrum, and Avrn to the normalized SPM average ("SPM Atlas"). Shaded regions delimit wavelength zones used for fitting as described in text.

of the difference in spectral resolution of the two instruments, while discrepancies at other wavelengths are due to differences in overall spectral response. We chose several wavelength zones well removed from line centers where, given equal spectral response, we would expect coincidence for both spectra and computed a low-order polynomial least-squares fit to the ratio using only points within the selected zones. We then divided the SPM average by this fit to produce the "SPM Atlas" (Figure 2.c) which has the same overall spectral behavior as the NSO Atlas.

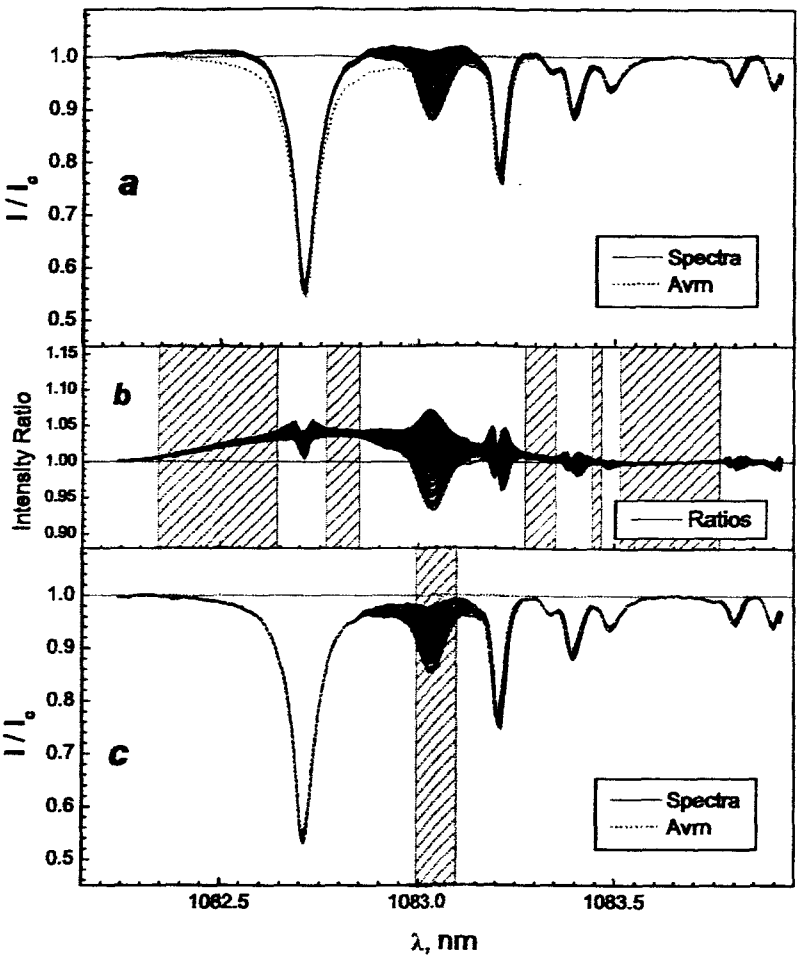

Figure 3. Normalization of individual spectra to average spectrum to define continuum with real spectral variation. Shaded regions delimit wavelength zones used for fitting as described in text.

To remove the SPM instrumental spectral response, we divided individual spectra (Figure 3.a) by the SPM Atlas. The resultant ratios (Figure 3.b) show strong solar variations near 1083 nm and the effects of shifts in telluric lines induced by our choice of a solar frame of reference, while differences at other wavelengths result mostly from non-linear instrumental response. We selected new wavelength zones which show little solar or telluric variation and, using only points within the zones, computed low-order polynomial least-squares fits to the ratios of each individual spectrum to the SPM Atlas. Finally, we divided the individual spectra by these instrumental response curves to obtain normalized spectra for subsequent analysis. The results, shown in Figure 3.c show

good overall agreement between the normalized spectra and the SPM Atlas spectrum, with differences primarily due to solar variations in the He multiplet. Note that most of the wavelength points used to determine the large-scale instrumental spectral response do not lie in regions of solar continuum. Application of this technique to a wider spatial field of view will require a spectral standard which includes center-to-limb variation.

We expect that this method for determining instrumental response from an independent spectral standard can be used to reduce spectra of other lines where no true continuum can be observed directly. The technique should also be useful for reducing 1083 nm observations from NSO's Synoptic Optical Long-term Investigations of the Sun (SOLIS) Vector Spectromagnetograph (VSM) whose bandpass is only about 1.0 nm. The danger in this technique is that any real variation in the selected zones will be misinterpreted as spectral response and will appear in the final data products as a false distortion of the spectrum in the region of interest. In the case of the He I 1083 nm multiplet, this precludes accurate treatment of certain high-velocity features (which are sometimes observed) unless they are identified prior to reduction and the affected spectral regions are excluded from the wavelength zones used to determine instrumental response.

To remove solar and telluric blends, we computed a multi-profile, least-squares fit to all major lines in the average spectrum and subtracted from this average the fitted curve of the He lines. The very weak water vapor line at 1083.03 nm identified by (Breckenridge and Hall, 1973) and the faint unidentified absorption features discussed by (Giovanelli and Hall, 1976) were not included in our least-squares fit. We then subtracted the result, an approximation of the average solar spectrum without He, from each individual spectrum to remove all other spectral features from the observations. We used the "Helium-less" average spectrum rather than its multi-line fit because residual fixed noise patterns which are common to both the average spectrum and each individual spectrum are thereby reduced or removed. This method of de-blending assumes that the wings of photospheric and telluric lines do not have noticeable variations in the spectral domain of the He I multiplet. This is a reasonable first approximation since we observed only a small central area of the disk where the primary solar variations occurred only in the He lines. The main effects of local Doppler velocities of the other solar lines were removed earlier in the reduction. To extend this method of differential blend removal to larger fields of view will require average spectra for several mean values of heliocentric position, and the method may not work well near the solar

limb. However, many improvements and variations of this method are possible and will be explored in future work.

We computed least-squares Gaussian fits to the normalized intensity profiles of the main two components of the He triplet. For this we used only wavelengths near line center as marked in Figure 3.c to avoid confusion with line asymmetry, blending with the minor component, and contamination by residual errors in removing other spectral features, primarily the Si I 1082.7 nm line. From the fit parameters, we computed

central intensity, $i_0 \equiv I_0/I_c \equiv 1 - d_0$, where d_0 is normalized line depth and all quantities are evaluated at line center, λ_0, as determined from the least-squares fit;

line-of-sight (Doppler) velocity, $v \equiv c(\lambda_0 - \bar{\lambda}_0)/\bar{\lambda}_0$, where $\bar{\lambda}_0$ is the spatially averaged line center position;

equivalent width $q \equiv \int [1 - i(\lambda)] d\lambda$; and

line width , w, such that $d(\lambda_0 \pm \bar{\lambda}_0 w/c)/d_0 = \exp(-1)$.

Line width, w, is computed in velocity units to reflect our feeling that the line broadening is primarily due to unresolved but non-thermal motions. Figure 4 presents images of each of these quantities. We visually identified from the intensity image rectangular areas containing a coronal hole, quiet Sun, a filament, and an active region. These are outlined and numbered on each of the four images in Figure 4. For reference, we have also over-plotted on each image intensity contours showing bright areas with relative central intensities exceeding 0.977.

3. Comparison with Paper I

To simplify the following discussion, we refer to the analysis technique presented above as MJ (Malanushenko and Jones). We have also analyzed the data from 17 April 2000 using the techniques exactly as presented in paper I, which we label J (Jones), and a variant thereof, which we label JV. We applied identical fixed-pattern correction, dark-current subtraction, and spatial averaging for all three methods. For method J, we determined the continuum by a low-order least-squares polynomial fit to intensities in several pseudo-continuum regions. We treated only the nearest strong lines, telluric water vapor at 1083.2 nm and the solar Si I line at 1082.7 nm for blend removal. To remove the telluric line, we divided the observed data by a reference profile which we derived from other observations in a coronal hole where the He multiplet was exceptionally weak and which we scaled by interpolation

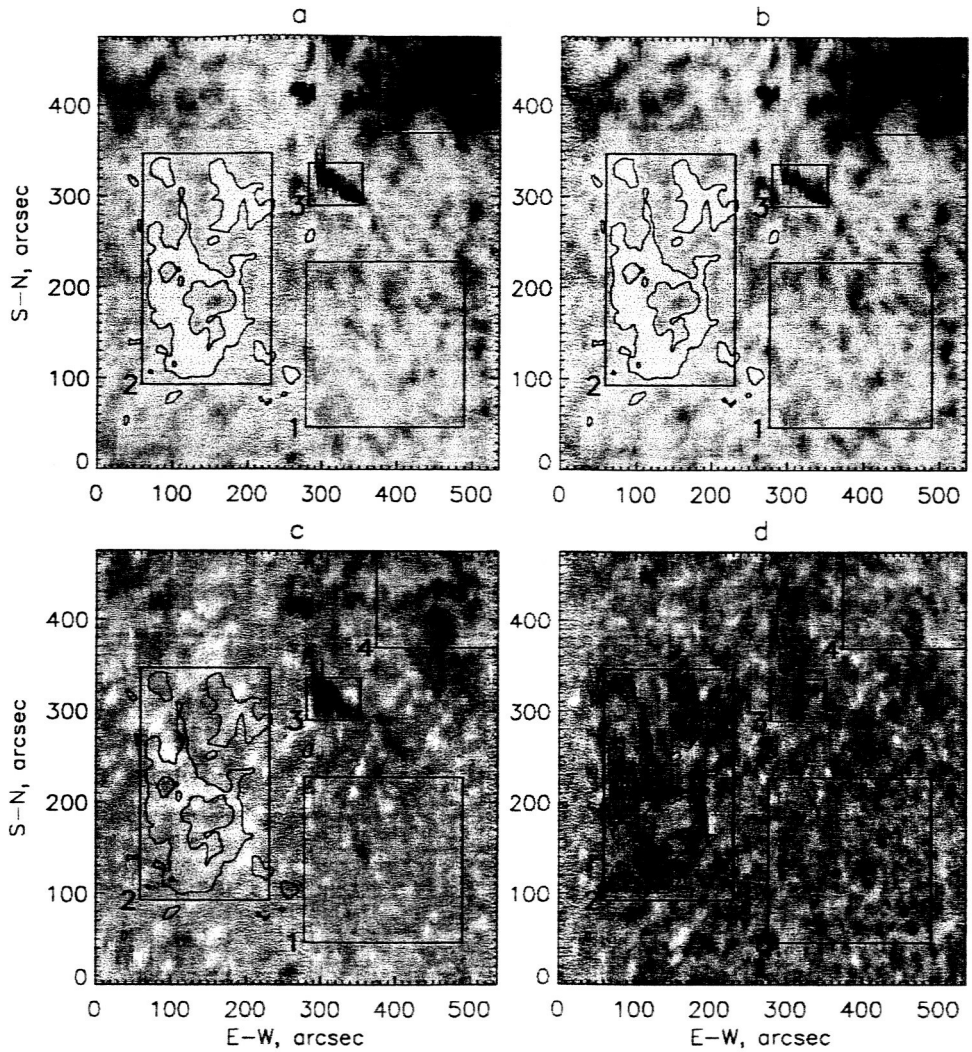

Figure 4. Images of i_0 (a), q (b), v (c), and w (d). Rectangles delineate quiet Sun (1), coronal hole (2), filament (3), and active region (4). The contour for $i_0 = 0.977$ is over-plotted on each image. Contrasts for grey-scales are linear with (black, white) levels for i_0 of (0.87, 0.99); for q of (140, 10 mÅ); for v of (-4.0, 4.0 km/s); and for w of (7.2, 18.0 km/s). Note that contrast is negative for q.

to match the observed Doppler width and line depth at each spatial position. We removed the Si I line by subtracting at every spatial position its least-squares spline fit symmetrized to match the blue wing, which is minimally blended with the He multiplet. (Giovanelli and Hall, 1976) used a similar method for treating the influence of the Si I line.

For method JV, we determined the continuum as in method MJ but removed the water vapor and Si I lines as in J.

For both methods J and JV, we computed i_0, v, q, and w using the rapid analysis technique of paper I which does not involve fitting any prescribed functional form to the observed He profiles. However, the "double-sided" determination of w as in paper I is sensitive to asymmetry and noise, particularly in the blue wing in coronal holes. To make w more comparable to the Gaussian fits of method MJ, we used the difference between the red-ward 1/e-line depth wavelength and line center rather than half the difference between the 1/e-points of both wings.

Figure 5 shows scatter plots comparing i_0, w, and v determined by methods MJ and JV as well as w determined by MJ and J. The plots are coded by color so that blue points are in the coronal hole, red in quiet sun, green in the active region, and black in the filament. One sees very good correspondence in central intensity between MJ and JV, while the other three comparisons are inferior. Most of this disagreement occurs in coronal holes and, less strongly, the quiet sun where small effects are amplified. As we illustrate below, the differences result almost entirely from variations in continuum determination and blend removal rather than in the method used to compute the various quantities.

We show in Figure 6 the result of continuum correction and blend removal for each of the three methods at a point within the coronal hole which we selected because the derived parameters were markedly discrepant. The top portion of Figure 6 shows the data normalized to the continuum for the three methods; in this case, JV and MJ are identical. The middle panel compares the normalized intensity with the fit to nearby lines for blend removal. The bottom panel compares the line depths found from the three methods. The continuum in method J is fixed by intensities in the wings of the Si and water vapor lines; this supresses any wings for the He lines and results in much smaller central line depth and line width than the other two methods. The fit to non-He lines in method MJ is influenced by remnants of the Gaussian fit to the He lines in the average profile and lies well above the fit determined by method JV. On the other hand, the resultant line depth is slightly smoother in method MJ since blend removal also reduces residual fixed pattern variation contained in the average profile. Simple inspection of the line-depth profiles in Figure 6 shows why, for this example, the central depths (or intensities) and positions for methods JV and MJ are similar but the line widths are very different. The actual technique for deriving the parameters from the given line profiles is not important for this comparison, and examination of profiles at other selected points suggests that this is the case throughout the image.

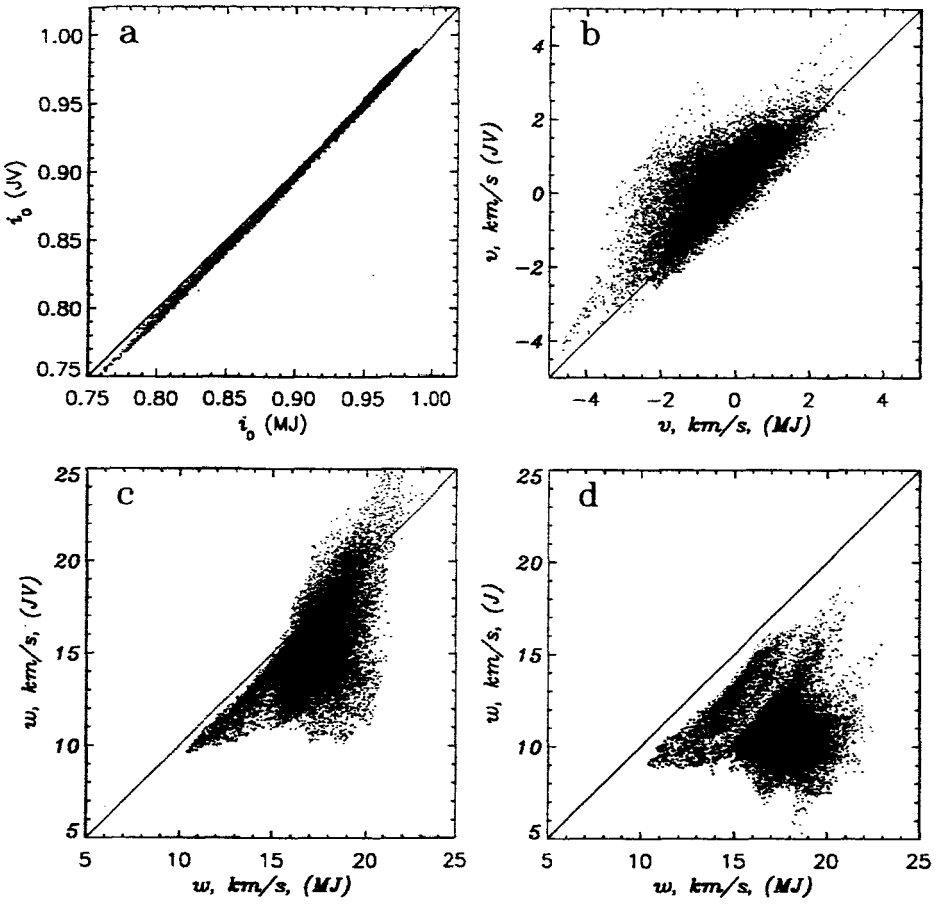

Figure 5. Scatter plots comparing i_0 (a), v (b) , and w (c) determined by methods MJ and JV as well as w (d) determined by MJ and J. Spatial points in quiet sun are colored red, coronal hole blue, active region green, and filament black. Horizontal axis in each case corresponds to method MJ.

The principal lesson to be drawn from this comparison is the extreme sensitivity of the results in coronal holes to the methods of reduction. Three reasonable methods can give dramatically different results since their differences, although small compared to the continuum, are significant fractions of the depth of the helium line. We believe that our analysis favors the current method of determining the continuum by correcting the instrumental response through comparison with a spectral standard. We are convinced that a hybrid method of blend removal, combining the advantages of MJ and JV, can be derived. Results presented in the remainder of this paper were derived by the MJ method. While we believe that they suggest interesting patterns of behavior, we

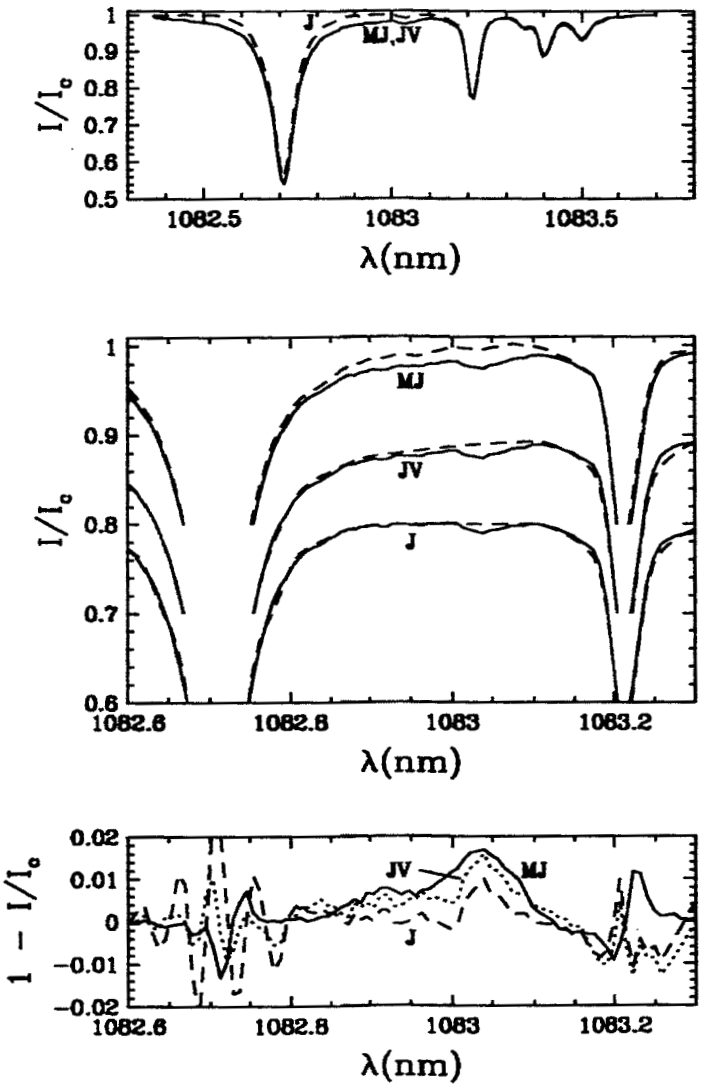

Figure 6. Continuum and de-blending for methods MJ, JV, and J. Top panel: data normalized by continuum as determined by JM,JV (solid) and J (dashed). Middle panel: normalized data (solid) and fits for de-blending (dashed); curves for JV and J have been displaced by -0.1 and -0.2 respectively. Bottom panel: normalized line depths for MJ (solid), JV (dotted), and J (dashed).

feel that the absolute values, particularly for line width and velocity in coronal holes, do not yet warrant a quantitative physical interpretation. Analysis of more data, including observations from different instruments where possible, is needed to make further progress.

4. Discussion

Figure 7 shows scatter-plots of v and w as functions of i_0 with points color coded by spatial region as in Figure 5. Since, as can be seen in Figure 4, the spatial distributions of i_0 and q are very similar, our results would be substantially the same for comparisons with q. The high correlation of central intensity (or line depth) with equivalent width has also been noted by others (Venkatakrishnan *et al.*, 1992). We organize our discussion of Figure 7 by spatial region.

4.1. Quiet Sun

The quiet Sun (region 1; red points in Figure 7) shows compact distributions in the cross-correlations of both v and w with i_0. In both cases, the correlation is negative, that is higher line widths and downward velocities are associated with lower central intensities or increased absorption. Similar correlation of w (with equivalent width instead of central intensity) was noted by (Venkatakrishnan *et al.*, 1992) who suggested that the variation of central intensity is caused by differences in external illumination and that the line widths are dominated by non-thermal motions. Our line widths are even larger than found by Venkatakrishnan *et al* (1992), and we agree that a non-thermal interpretation is required. However, we also find a much smaller range in line width ($\approx$ 30% in our case vs a factor of two in Venkatakrishnan *et al*,1992). We suspect that the discrepant values and ranges of line width stem primarily from Venkatakrishnan *et al.*'s choice of continuum which corresponds to a simplified version of method J above, with no explicit correction for blends.

We agree with the inference by (Venkatakrishnan *et al.*, 1992) that increased absorption (near cell boundaries) in the quiet Sun is caused by increased external illumination rather than local properties of the boundaries themselves. However, our reasoning is quite different. Standard one-dimensional models of active regions and cell boundaries (see Fontenla *et al.*,1999) cannot produce the observed strengthening *without* increased external radiation. In these models, the height of the rapid transition-region temperature rise, where He photoionization- recombination becomes effective, lowers with increasing activity, and thus the density of this region increases. Although this sequence of temperature structures reproduces other observed spectral features, the resultant increase of collisional transitions from the triplet to singlet series of He I, which are overwhelmingly followed by radiative transitions (58.4 and 53.7 nm) to the singlet ground state, de-populates the energy levels involved in 1083 nm formation (Andretta and Jones, 1997). Thus, in

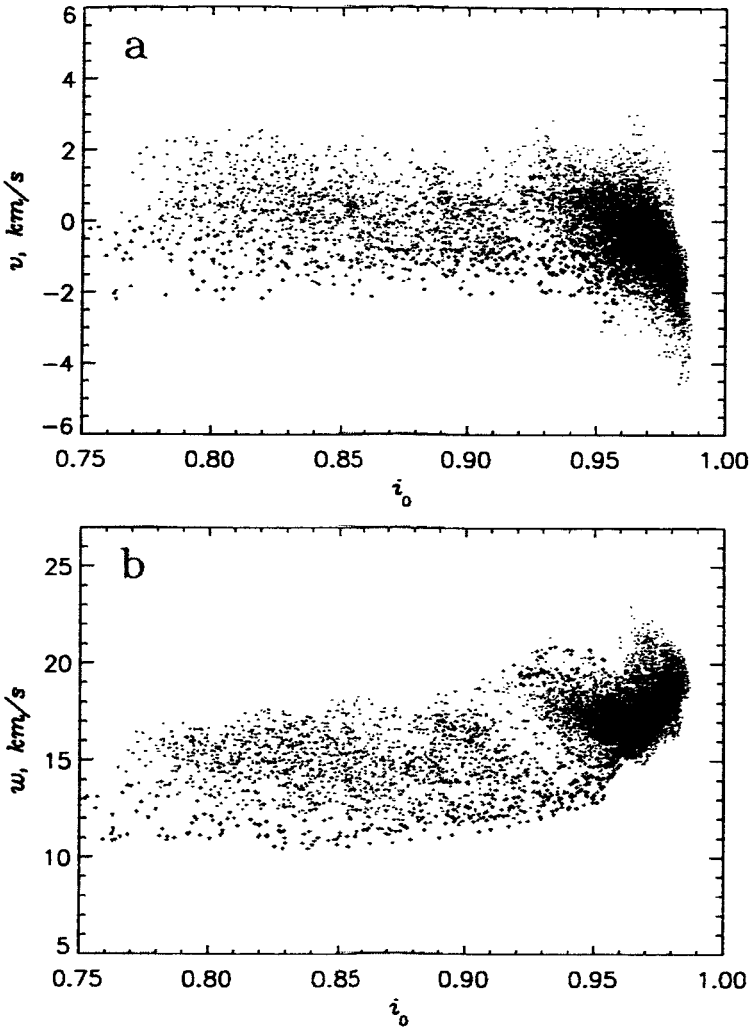

Figure 7. Scatter-plots of Doppler velocity v (a) and line width w (b) with relative central intensity i_0. Red corresponds to quiet Sun, black to filament, green to active region, and blue to coronal hole.

the absence of changing external illumination, He 1083 nm absorption decreases with increasing activity (Avrett *et al.*, 1994) as a result of density *increases*. In contrast, (Venkatakrishnan *et al.*, 1992) argue that lateral pressure balance implies reduced density in regions of high magnetic field, and infer, wrongly in our opinion, that the lowered density alone would reduce 1083 nm absorption.

We observe the opposite sense of correlation of v with 1083 nm absorption than found by Venkatakrishnan *et al* (1992). That is, we

observe increased outward velocities in areas of weaker absorption (cell interiors) and downward velocities in areas of stronger absorption (network boundaries). We see no obvious explanation of the discrepancy except that the systematic errors in the two studies are quite different due to differing choices of continuum and methods of observation (they scan in wavelength with potential confusion of temporal and spectral information).

Our range of central intensities in the quiet Sun agrees well with the results of (Giovanelli and Hall, 1976) who also examine center-to-limb behavior and compare their results with simple geometric models of the line-forming region in cell boundaries. They conclude that He I 1083 nm absorption is spatially unresolved in cell boundaries, but our analysis does not directly address this issue.

4.2. Coronal Hole

In the coronal hole (region 2; blue points in Figure 7), we note the overlap in intensity range between coronal hole and quiet Sun, a fact which greatly complicates identification of coronal holes based on central intensity or equivalent width alone. Only the very brightest (lowest absorption) regions of the coronal hole lie outside the quiet-Sun range. We note that the presence of a normally faint telluric water vapor line at 1083 nm can shift the range of coronal-hole central intensities even more into the quiet-Sun range on days with moderate to high humidity.

The correlation of v with i_0 is negative as in the quiet Sun, implying that the centers of network cells have preferential outward motions. Much of the correlation distribution for the coronal hole overlaps that for the quiet Sun, but the brightest (lowest absorption) regions of the coronal hole tend to higher outward velocities ($\approx$ 4 km/s). A similar spatial pattern of excess blue-wing absorption was seen by Dupree, Penn and Jones (1996), although the inferred velocities were higher and the effect was not observed in central line shift. Again, the method of continuum determination in Dupree, Penn and Jones (1996) was similar to method J (where systematic outward velocities in the coronal hole were not apparent) and Venkatakrishnan *et al* (1992). Belkina *et al.* (1997) inferred differential outflow of order 1.0 km/s between coronal holes and quiet sun using 1083 nm spectroheliograms in the centers and wings of the He line but they could not distinguish network centers and boundaries for quiet Sun. We note that in our case, the velocities in coronal-hole cell centers are the least accurately determined, and further progress depends upon more and better data.

An important feature of the coronal hole correlations is the positive association of line width and central intensity, in the opposite sense

to the quiet Sun, even though the ranges where both w and i_0 are similar. To our knowledge, this effect has not been observed by other researchers, and we will explore its application for coronal hole identification in future papers. The opposite correlation suggests that either the physical character of chromospheric network or the mechanism of He 1083 nm line formation therein is not the same in quiet Sun and coronal holes.

Broadening of spectral lines in coronal holes are also observed in in TR (Lemaire et al., 1999; Stucki *et al.*, 2000) and in the corona (Wilhelm *et al.*, 1998; Grammer *et al.*, 1999). Although beyond the scope of this paper, broadening of the He I 1083 nm multiplet in coronal holes may provide important constraints on the height distribution of the solar wind acceleration as a lower boundary condition. However, we note from the discussion in section 3 that the absolute value of our derived line widths is most dependent on the reduction method in precisely these low-absorption regions, so that further observations and analysis are needed to confirm this result.

4.3. Filament

The region of interest includes the small filament and some area of i_0 similar to quiet Sun (region 3 in 4 Figure; black points in Figure 7). Part of this area appears in Figure 7 as black points superimposed on the quiet-Sun correlations. However, a closer inspection of Figure 4 shows that the filament appears larger in w than in i_0. This can be seen in Figure 7 as points which are both narrower and show motions with an outward bias at the same levels as the darker portions of the filament. Excluding the quiet-Sun points within region 4, neither v or w show systematic trends with i_0. That the filament is narrower than the surroundings suggests less turbulence; it is difficult to comment on the apparent velocity structure without knowledge of its temporal behavior. We have no explanation for the appearance of points with velocities and line widths which are apparently associated with the filament but whose central intensities are typical of quiet Sun.

4.4. Active Region

The active region (region 4; green points in Figure 7) shows an extended range of central intensity variation with central line depths exceeding quiet-Sun and coronal-hole values by as much as an order of magnitude (cf. Venkatakrishnan *et al.* 1997). At lower central intensities, the quality of our Gaussian fits begins to deteriorate, perhaps indicating that the optically thin assumption is beginning to fail as suggested by Venkatakrishnan *et al.* (1997); however, the line is sufficiently deep

that errors in specifying the continuum become small. We see little systematic dependence of either v or w on central intensity. The former might be expected in the quasi-stationary decaying phase of an active region, while the latter is somewhat at variance with the results of Venkatakrishnan *et al.* (1997) who report a slight trend of increasing width with increasing absorption. Lower line widths in active regions are commonly observed in UV and EUV lines and are accounted for in the FAL models by increasingly truncated chromospheric temperature plateaus with increasing activity. We note that the section of active region which we analyzed is small and may not be representative.

5. Summary

We have developed a new technique for normalizing He I 1083 nm spectroscopy using a well calibrated standard and applied it to an example of imaging spectroscopy obtained with the NSO/KPVT Spectromagnetograph. We compare the technique with other methods of reduction and find that the methods used to determine the continuum and remove the effects of blends greatly affects line profiles and parameters derived from them in coronal holes and in the centers of quiet-Sun network.

Our analysis indicates that Doppler velocity is negatively correlated with central line intensity in quiet Sun and coronal holes but shows little systematic trend in the active region and filament. We find marginal indication of preferential out-flows within the coronal hole. Line width is also negatively correlated with central intensity in the quiet Sun but is both systematically larger and positively correlated with intensity in coronal holes. Line widths also show little variation with intensity in the active region and filament and are of similar or smaller magnitude to that in the quiet Sun. The filament shows preferential outflow and reduced line width, and we observe in both correlation plots and images that there are regions which seem associated with the filament in Doppler velocity and line width but are not distinguishable from quiet Sun in central intensity.

In future work we will improve our analysis method and extend the analysis to many data sets.

Acknowledgements

NSO/Kitt Peak data used here are produced cooperatively by NSF/NOAO, NASA/GSFC, and NOAA/SEC. This work was supported by NASA Office of Space Sciences grant 344-12-51-14.

We thank W. Livingston and M. Penn for valuable discussions.

References

Andretta V., Jones H.P.: 1997, *Astrophys. J.* **489**, 375.

Avrett, E.N., Fontenla, J.M. and Loeser, R.: 1994, IAU Symp. 154, *Infrared Solar Physics*, D.M Rabin *et al.* ed., 35.

Belkina, I. L.; Akimov, L. A.; Beletsky, S. A.; Korokhin, V. V.; Marchenko, G. P.: 2000, *Kinematika i Fizika Nebesnykh Tel* **16**, 316.

Breckenridge, J.B. and Hall, D.N.B.: 1973, *Solar Phys.* **28**. 15.

Dupree, A.K., Penn, M.J. and Jones, H.P.: 1996, *Astrophys. J.*, **467** L121.

Elmore, D.F., Card, G.L., Chambellan, C.W., Hassler, D.M., Hull, H.L., Lecinski, A.R., MacQueen, R.M., Streander, K.V., Streete, J.L., and White, O.R.: 1998, *Applied Optics.* **37**, 4270.

Fontenla, Juan; White, Oran R.; Fox, Peter A.; Avrett, Eugene H.; Kurucz, Robert L.: 1999, *Astrophys. J* **518**, 480.

Gilbert, H.R. and Holzer, T.E.: 2002, Amer. Geophys. Union Fall Meeting abstract SH52A-0438.

Giovanelli, R.G. and Hall, D.: 1976, *Solar Phys.* **52**, 211.

Golub, L., Harvey, K.L., Herant, M., and Webb, D. F.: 1989, *Solar Phys.* **124**, 211.

Grammer S.R., Kohl J.L., Noci G.: 1999, *Astrophysical Journal*, **511**, 481.

Harvey, K.L.: 1994, IAU Symp. 154, *Infrared Solar Physics*, D.M Rabin *et al.* ed., 71.

Harvey, K.L and Recely, F.:2002, *Solar Phys.* **211**, 31.

Jones, H.P.: 1994, IAU Symp. 154, *Infrared Solar Physics*, D.M Rabin *et al.* ed., 49.

Jones, H.P.: 2003, *Solar Phys.* **218**, 1. (Paper I)

Jones, H. P., Duvall, T. L. Jr., Harvey, J. W., Mahaffey, C. T., Schwitters, J. D., Simmons, J. E.: 1992, *Solar Phys.* **139**, 211.

Lemaire, P., Bocchialini K., Aletti, V.: 1999, *Space Sci. Rev.*, **87**, 249.

Livingston, W. C., Harvey, J., Pierce, A. K., Schrage, D., Gillespie, B., Simmons, J., Slaughter, C.: 1976, *Applied Optics.* **15**, 33.

Malanushenko, V.P., Polosukhina, N.S. and Weiss, W.W.: 1992, *Astronomy and Astrophysics* **46**, 73.

Singh, J.; Jain, S. K.; Venkatakrishnan, P.:1994 *Solar Physics*, **150**, 49.

Stepanian, N. N.; Dolgopolova, E. V.; Elizarov, A. I.; Malanushenko, E. V.; Parchevskii, K. V.; Sunitsa, G. A.: 2000, *Bull. of the Crimean Astrophysical Observatory*, **96**, p. 171.

Stucki, K.; Solanki, S. K.; Schuhle, U.; Ruedi, I.; Wilhelm, K.; Stenflo, J. O.; Brkovic, A.; Huber, M. C. E. : 2000, *Astron. Astrophys.*, **363**, 1145.

Venkatakrishnan, P.; Jain, S. K.; Singh, Jagdev; Recely, F.; Livingston, W. C.: 1992, *Solar Physics*, **138**, March, 107.

Venkatakrishnan, P.; Sakurai, T.; Suematsu, Y.; Ichimoto, K.: 1997, *Bull. Astr. Soc. India*, **25**, 527.

Wallace, L., Hinkle, K., Livingston, W.: 1993, *N.S.O. Technical Report* **#93-001**, Published April, 1993 by National Solar Observatory.

Wilhelm, K., Marsch, E., Dwivedi, B.N., Hassler, D.M., Lemaire, P., Gabriel, A.H., Huber, M.C.E.: 1998, *Astrophysical Journal*, **500**, 1023.